Fluorescence modeling for optimized-binary compressive detection Raman spectroscopy

Owen G. Rehrauer,[1] **Bharat R. Mankani,**[1] **Gregery T. Buzzard,**[2] **Bradley J. Lucier,**[3] **and Dor Ben-Amotz**[1,*]

[1]*Purdue University, Department of Chemistry, West Lafayette, IN, USA*
[2] *Purdue University, Department of Mathematics, West Lafayette, IN, USA*
[3]*Purdue University, Departments of Mathematics and Computer Science, West Lafayette, IN, USA*
[*]*bendor@purdue.edu*

Abstract: The recently-developed optimized binary compressive detection (OB-CD) strategy has been shown to be capable of using Raman spectral signatures to rapidly classify and quantify liquid samples and to image solid samples. Here we demonstrate that OB-CD can also be used to quantitatively separate Raman and fluorescence features, and thus facilitate Raman-based chemical analyses in the presence of fluorescence background. More specifically, we describe a general strategy for fitting and suppressing fluorescence background using OB-CD filters trained on third-degree Bernstein polynomials. We present results that demonstrate the utility of this strategy by comparing classification and quantitation results obtained from liquids and powdered mixtures, both with and without fluorescence. Our results demonstrate high-speed Raman-based quantitation in the presence of moderate fluorescence. Moreover, we show that this OB-CD based method is effective in suppressing fluorescence of variable shape, as well as fluorescence that changes during the measurement process, as a result of photobleaching.

OCIS codes: (300.6450) Spectroscopy, Raman; (120.6200) Spectrometers and spectroscopic instrumentation; (070.6120) Spatial light modulators.

References and links

1. J. W. Chan, D. S. Taylor, T. Zwerdling, S. M. Lane, K. Ihara, and T. Huser, "Micro-Raman spectroscopy detects individual neoplastic and normal hematopoietic cells," Biophys. J. **90**, 648–656 (2006).
2. A. M. K. Enejder, T.-W. Koo, J. Oh, M. Hunter, S. Sasic, M. S. Feld, and G. L. Horowitz, "Blood analysis by Raman spectroscopy," Opt. Lett. **27**, 2004–2006 (2002).
3. O. O. Soyemi, F. G. Haiback, P. J. Gemperline, and M. L. Myrick, "Nonlinear optimization algorithm for multivariate optical element design," Appl. Spectros. **56**, 477–487 (2002).
4. M. F. Duarte, M. A. Davenport, D. Tarkhar, J. N. Laska, T. Sun, K. F. Kelly, and R. G. Baraniuk, "Single-pixel imaging via compressive sampling," IEEE Signal Process. Mag. **25**, 83–101 (2008).
5. W. C. Sweatt, C. A. A. Boye, S. M. Gentry, M. R. Descour, B. R. Stallard, and C. L. Grotbeck, "ISIS: an information-efficient spectral imaging system," Proc. SPIE **3438**, 98–106 (1998).
6. N. Uzunbajakava, P. de Peinder, G. W. t Hooft, and A. T. M. van Gogh, "Low-cost spectroscopy with a variable multivariate optical element," Anal. Chem. **78**, 7302–7308 (2006).
7. J. E. Vornehm, A. J. Dong, R. W. Boyd, and Z. Shi, "Multiple-output multivariate optical computing for spectrum recognition," Opt. Express **21**, 25005–25014 (2014).

8. D. S. Wilcox, G. T. Buzzard, B. J. Lucier, P. Wang, and D. Ben-Amotz, "Photon level chemical classification using digital compressive detection," Anal. Chim. Acta **755**, 17–27 (2012).

9. D. S. Wilcox, G. T. Buzzard, B. J. Lucier, O. G. Rehrauer, P. Wang, and D. Ben-Amotz, "Digital compressive chemical quantitation and hyperspectral imaging," Analyst **138**, 4982–4990 (2013).

10. G. T. Buzzard and B. J. Lucier, "Optimal filters for high-speed compressive detection in spectroscopy," Proc. SPIE **8657**, 865707 (2013).

11. J. Zhao, H. Lui, D. I. McLean, and H. Zeng, "Automated autofluorescence background subtraction algorithm for biomedical Raman spectroscopy," Appl. Spectrosc. **61**, 1225–1232 (2007).

12. C. A. Lieber and A. Mahadevan-Jansen, "Automated method for subtraction of fluorescence from biological Raman spectra," Appl. Spectrosc. **57**, 1363–1367 (2003).

13. D. V. Martyshkin, R. C. Ahuja, A. Kudriavtsev, and S. B. Mirov, "Effective suppression of fluorescence light in Raman measurements using ultrafasttime gated charge coupled device camera," Rev. Sci. Instrum. **75** 630–635 (2004).

14. N. Everall, R. W. Jackson, J. Howard, and K. Hutchinson, "Fluorescence rejection in Raman spectroscopy using a gated intensified diode array detector," J. Raman Spectrosc. **17** 415–423 (1986).

15. N. J. Everall, J. P. Partanen, J. R.M. Barr and M. J. Shaw, "Threshold measurements of stimulated Raman scattering in gases using picosecond KrF laser pulses," Opt. Commun. **64** 393–397 (1987).

16. D. Zhang and D. Ben-Amotz "Enhanced chemical classification of Raman images in the presence of strong fluorescence interference," Appl. Spectrosc. **54** 1379–1383 (2000).

17. F. Pukelsheim, *Optimal design of experiments*, (John Wiley & Sons Inc. 1993).

18. A. C. Atkinson, A. N. Donev, and R. D. Tobias, *Optimum experimental designs with SAS*, (Oxford University Press, 2007).

19. K. Golcuk, G. S. Mandair, A. F. Callender, N. Sahar and D. H. Kohn and M. D. Morris, "Is photobleaching necessary for Raman imaging of bone tissue using a green laser?" BBA - Biomembranes **1758**, 868–873 (2006).

20. S. Bernstein, "Demonstration du theoreme de weierstrass fondee sur le calcul des probabilities," Comm. Soc. Math. Kharkov **13**, 1–2 (1912).

21. R. T. Farouki, "The Bernstein polynomial basis: a centennial retrospective," Comput. Aided Geom. Design **29**, 379–419 (2012).

22. C. Frausto-Reyes, C. Medina-Gutiérrez, R. Sato-Berrú, and L. R. Sahagún, "Qualitative study of ethanol content in tequilas by Raman spectroscopy and principal component analysis," Spectrochim. Acta A **61**, 2657–2662 (2005).

23. R. Sato-Berrú, J. Medina-Valtierra, C. Medina-Gutiérrez, and C. Frausto-Reyes, "Quantitative NIR Raman analysis in liquid mixtures," Spectrochim. Acta A **60**, 2225–2229 (2004).

1. Introduction

Current spectroscopic chemical analysis instruments are capable of generating data sets that are so large that they require transforming the data to a lower-dimensional space, using methods such as principal component analysis (PCA) [1] or partial-least squares (PLS) [2] to facilitate subsequent automated chemical classification and quantitation. Moreover, because the collection of high-dimensional data is often the slowest step in the process, a number of compressive detection strategies [3–7] have been introduced with the goal of increasing data collection speed by making measurements only in the low-dimensional space containing the information of interest. One such method is our previously described optimized binary compressive detection (OB-CD) strategy, in which OB filters are applied to a digital mirror microarray (DMD) to redirect or collect photons of (multiple) selected colors, for detection using a single channel detector, such as a photon counting photomultiplier tube (PMT) or an avalanche photodiode (APD) [8, 9].

Previously [8–10], we demonstrated that the OB-CD strategy enabled high-speed chemical classification, quantitation, and imaging. Here we demonstrate an extension of the OB-CD method that facilitates Raman classification and quantitation in the presence of fluorescence background. Key advantages of this method, relative to conventional fluorescence subtraction strategies [11–16], include its compatibility with automated high-speed chemical analysis in the presence of variable fluorescence backgrounds. Here we show that fluorescence backgrounds may be quantified and subtracted on-the-fly by including Bernstein polynomial spectral functions in the OB-CD training set, along with Raman spectra of the components of interest. In

other words, we augment the Raman spectral training set with Bernstein polynomial spectral shapes to model fluorescence and thus obtain OB-CD filters that are used to quantify both the chemical components of interest and the fluorescence background spectra.

2. Theory

We begin by giving a short summary of the OB-CD mathematical framework [8]; some of the wording is taken from the cited paper and we refer the reader there for more details and discussion, including our assumption of linear additive spectra, which justifies in part the form of our model. This framework is based on the subfield of statistics known as "Optimal Design of Experiments" [17]. We then discuss the notion of *nuisance parameters* and how this notion can be exploited to reduce the variance of the estimated photon emission rates pertaining to the (non-nuisance) components of interest. Finally, we introduce a new strategy for modeling, quantifying, and suppressing fluorescence background signals in Raman spectra.

2.1. Review of mathematical model

We assume that our chemical sample consists of a mixture of n known chemical species S_j, $j = 1, \ldots, n$. In a particular sample, the species S_j emits photons at a rate Λ_j, so the number of photons emitted in time t is a Poisson random variable with mean $t\Lambda_j$; our goal is to estimate these rates as accurately as possible, in order to quantify the composition of a sample containing such components.

The wavelength, or energy, of each photon observed in the experiments can be labeled with an integer $i \in \{1, \ldots, N\}$. Assume that we know the shape of the spectrum associated with species S_j; denote the probability that a photon from species S_j has label i by P_{ij}, so $\sum_{i=1}^{N} P_{ij} = 1$. In other words, the P_{ij}, $i = 1, \ldots, N$, form the spectrum of the jth compound, normalized so that the sum is 1. Thus the stream of labeled photons emanating from a sample is modeled by a vector Poisson process with rates $P\Lambda$, where $\Lambda = (\Lambda_1, \ldots, \Lambda_n)^T$, and $P = (P_{ij})_{N \times n}$. (Here and later, superscript T denotes "transpose.") If we measure the number of photons that arrive in each energy bin for time t then the number of photons with label i entering our instrument from all chemical species has a Poisson distribution with mean $t(P\Lambda)_i = t\sum_{j=1}^{n} P_{ij}\Lambda_j$. We assume that the number of wavelength channels, N, is greater than the number of chemical species n, and that the columns of P are linearly independent, i.e., P has full rank. (In other words, we assume that no spectrum can be written as a linear combination of the other spectra.)

We consider taking m independent measurements with $m \geq n$. In the kth measurement, we set in our *optical filter* the transmittance of all photons with energy level i to be a number F_{ik} with $0 \leq F_{ik} \leq 1$; i.e., the probability that in the kth measurement a photon with energy label i is counted is F_{ik}. Our observation in the kth measurement is the total photon count, summed over all energy levels i, from observing the photon stream for time T_{kk}, which will be a Poisson random variable with mean

$$T_{kk} \sum_{i=1}^{N} F_{ik} \left(\sum_{j=1}^{n} P_{ij}\Lambda_j \right) = T_{kk} \sum_{i=1}^{N} \sum_{j=1}^{n} F_{ik} P_{ij}\Lambda_j.$$

(We use a double subscript on T_{kk} because we will make these numbers the diagonal of a matrix T.) We refer to the columns of the matrix $F = (F_{ik})_{N \times m}$ as *filters*, and the entries of F can be chosen as we wish, since they are parameters of our measuring device. Based on [17] and as in [8], we choose filters F and corresponding measurement times T to minimize the variance in estimated rates, subject to a total time constraint expressed as $\sum_{k=1}^{m} T_{kk} = 1$.

For a DMD, we can choose only $F_{ik} = 0$ or $F_{ik} = 1$, while for an analog spatial light modulator (SLM) we can in principle choose any $0 \leq F_{ik} \leq 1$. (Moreover, one could use a DMD as an

analogue filter by varying time for which each individual energy bin in a given filter is turned on, although we have not done so in the present studies.)

We denote by $\mathbf{x}$ our complete observation, a vector of m independent Poisson random variables with means and variances given by the vector $TF^TP\Lambda$, where T is the $m \times m$ diagonal matrix with diagonal entries $T_{11},\ldots,T_{mm}$ and F^TP is an $m \times n$ matrix. We assume that F is chosen so that F^TP has rank n (which is possible since P has rank n and $m \geq n$).

If we denote by $\hat{\mathbf{x}}$ a sample from this random variable, then our estimate $\hat{\Lambda}$ of the true rates Λ is given by $\hat{\Lambda} = BT^{-1}\hat{\mathbf{x}}$, where the $n \times m$ matrix $B = (b_{ik})_{n \times m}$ is a *left inverse* of F^TP, i.e., $B(F^TP) = I$, the $n \times n$ identity matrix. (If $n = m$ then F^TP is a square matrix and B is simply $(F^TP)^{-1}$.) We note that the expected value of $\hat{\Lambda}$ satisfies $E(\hat{\Lambda}) = BT^{-1}E(\hat{\mathbf{x}}) = BT^{-1}(TF^TP\Lambda) = \Lambda$, so $\hat{\Lambda}$ is an unbiased estimator of Λ.

It was shown earlier [8] that the variance of the estimate $\hat{\Lambda}_j$ of the jth rate Λ_j is given by

$$E\left(|(BT^{-1}\mathbf{x})_j - \Lambda_j|^2\right) = \sum_{k=1}^{m} b_{jk}^2 T_{kk}^{-1}(F^TP\Lambda)_k.$$

In the cited paper the variances were summed over *all* Λ_j to derive

$$E\left(\|BT^{-1}\mathbf{x} - \Lambda\|^2\right) = \sum_{j=1}^{n}\sum_{k=1}^{m} b_{jk}^2 T_{kk}^{-1}(F^TP\Lambda)_k = \sum_{k=1}^{m} \frac{((F^TP)\Lambda)_k}{T_{kk}}\|B\mathbf{e}_k\|^2. \quad (1)$$

Here $\mathbf{e}_k$ is a vector whose components are zero except for a 1 in the kth component and $\|y\|^2 = \sum_{j=1}^{n} y_j^2$.

We now deviate a bit from the earlier exposition [8], where it is perhaps not stated clearly that because the sum of variances (1) depends on the unknown rates Λ, we cannot choose $m, F, T,$ and B to minimize (1) for *all* Λ simultaneously. Therefore we pick a single $\bar{\Lambda} = (1,\ldots,1)^T$ and choose $m, F, T,$ and B to minimize

$$E\left(\|BT^{-1}\mathbf{x} - \bar{\Lambda}\|^2\right) = \sum_{k=1}^{m} \frac{((F^TP)\bar{\Lambda})_k}{T_{kk}}\|B\mathbf{e}_k\|^2 \quad (2)$$

under the constraints $m \geq n$; $0 \leq F_{ik} \leq 1$, $1 \leq i \leq n$, $1 \leq k \leq m$; $0 < T_{kk}$, $1 \leq k \leq m$, and $\sum_{k=1}^{m} T_{kk} = 1$; and $B(F^TP) = I$. This choice of $\bar{\Lambda}$ has proved useful absent additional information [8]. Our experience indicates that the resulting filters and measurement times are relatively insensitive to changing individual coefficients in $\bar{\Lambda}$ by up to a factor of 100.

2.2. Nuisance parameters

It often happens that the photon emission rates of some chemical species are of more interest than others. One might have a contaminant with a broad (known) spectrum; while this may be one of the chemical species S_j, we don't really care about the accuracy of estimation of that particular Λ_j. In the field of Optimal Design of Experiments, such variables Λ_j are known as *nuisance parameters*: They are a necessary part of the model, but we don't care about the accuracy of their estimates except insofar as it affects the estimates of the other variables [18].

We assume that we are truly interested in the photon emission rates of only the first $n' < n$ chemical species. For such systems, we don't care about the variances of the estimates of Λ_j for $n' < j \leq n$ and so instead of minimizing (2) we minimize the sum of the variances of of the estimates of only the first n' emission rates:

$$\sum_{j=1}^{n'} E\left(|(BT^{-1}\mathbf{x})_j - \bar{\Lambda}_j|^2\right) = \sum_{j=1}^{n'}\sum_{k=1}^{m} b_{jk}^2 T_{kk}^{-1}(F^TP\bar{\Lambda})_k.$$

In effect, we estimate Λ_j for $n' < j \leq n$ only well enough to minimize the error of the sum of variances of the first n' emission rates.

2.3. Estimating fluorescence using Bernstein polynomials

A fluorescent spectrum is generally smooth and broad, in contrast to the narrow peaks found in Raman spectra; it may vary from one sample to another, or from time to time for the same sample.

One can reduce the amount of fluorescence in a sample by photobleaching the sample prior to analysis [19]. Another commonly-used procedures for subtracting such fluorescence backgrounds from Raman spectra is to fit the fluorescent spectrum to a polynomial [11,12]; in effect, this amounts to using a fixed polynomial of specified degree to model a fluorescent spectrum. This may work well if in a set of samples the fluorescence doesn't vary over space or time; this is often not the case, however, in Raman (and particularly Raman imaging) applications, for which one must estimate the shape of the fluorescence dynamically.

Instead of somehow applying conventional fluorescence fitting and subtraction strategies to OB-CD measurements, we use OB-CD filters that are derived using either actual fluorescence spectra of known shape or a family of polynomials that models general fluorescence spectra.

More specifically, if the sample of interest contains a fixed fluorescent signal of known shape, we do the following. We simply add the fluorescence spectrum as an extra column of P with associated rate variable Λ_j, and then treat Λ_j as a nuisance parameter, not adding its variance to the sum of variances being minimized.

If the fluorescence has a spectrum that varies over space or time, however, we cannot apply the previous procedure and must model the fluorescence dynamically, as follows.

Since fluorescence backgrounds can often be fit reasonably well by a cubic polynomial, we would like to identify a polynomial basis for cubic polynomials such that (1) all basis elements are nonnegative on $[0,1]$ and (2) every nonnegative polynomial can be written as a linear combination of the basis elements with nonnegative coefficients. (Negative coefficients, which are supposed to model rates, are nonphysical and increase the variance of our estimates.) Unfortunately, for $r > 1$, no such basis exists.

Of interest, however, is the *Bernstein basis* [20, 21] of polynomials of degree r, given by

$$B_{v,r}(x) = \binom{r}{v} x^v (1-x)^{r-v}, \quad v = 0, 1, \ldots, r,$$

are nonnegative on $[0,1]$ (so any linear combination of them with nonnegative coefficients is nonnegative on $[0,1]$). They have other nice properties: They form a basis for the space of polynomials of degree r; they have optimal stability is some sense [21]; and "many" if not "most" nonnegative polynomials that come up in practice as models for fluorescent spectra have nonnegative coefficients in the Bernstein basis (or at least, any negative coefficients are not "overly" large). The Bernstein polynomials even resemble single-peak spectra.

In the specific case $r = 3$ we have $B_{0,3}(x) = (1-x)^3$, $B_{1,3}(x) = 3x(1-x)^2$, $B_{2,3}(x) = 3x^2(1-x)$, $B_{3,3}(x) = x^3$. These polynomials are shown in Fig. 1.

In this work we model fluorescent spectra with linear combinations of $B_{v,3}(x)$, $v = 0,1,2,3$, and often treat the Bernstein coefficients as nuisance parameters. Because fluorescent spectra are not precisely polynomials, this introduces *model error*, which we discuss in the Results and Discussion section. We have also found that for some purposes using quartic polynomials ($r = 4$) gives more accurate results.

3. Methods and materials

3.1. OB-CD spectrometers

We have previously described an OB-CD spectrometer using a 785 nm laser for excitation with 75 mW at the sample [8]. In the present studies we have utilized that spectrometer as well as
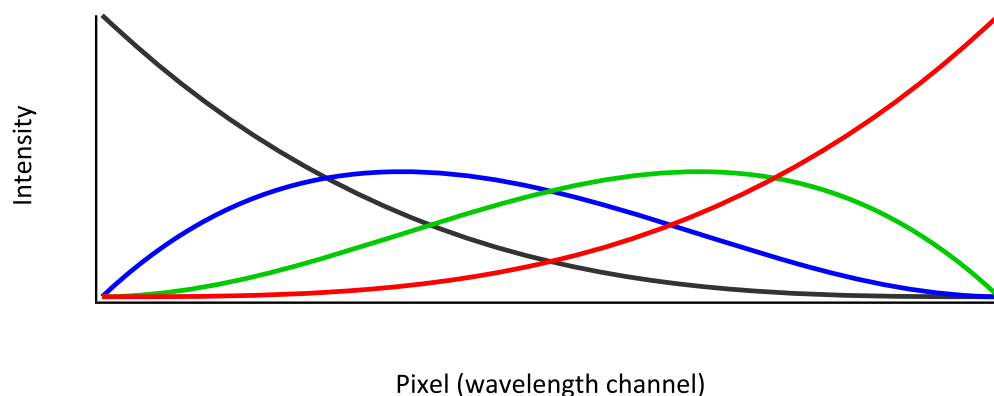
Fig. 1. Plot of the four degree-three Bernstein polynomials as a function of wavelength channel (scaled to be over the interval $[0,1]$.) The colors denote the various polynomials: black, $B_{3,0}(x)$; blue, $B_{3,1}(x)$; green, $B_{3,2}(x)$; and red, $B_{3,3}(x)$.

a new OB-CD spectrometer using a 514 nm laser for excitation whose schematic is shown in Fig. 2 (the 785 nm excitation laser system is similar in design, as previously described in [8]). Much like the previously described system, our microscope is configured to collect the back-scattered Raman signal with the same objective lens that is used to focus the argon ion laser (Modu Laser Stellar Pro L 100 mW) onto the sample. The laser passes through a laser-line bandpass filer (Semrock RazorEdge) before it is focused onto the sample using a microscope objective (Nikon MPlan, 20x, 0.4 NA), and unless indicated otherwise the laser power at the sample was about 12 mW for all experiments described in this paper. The backscattered light is collected and then separated from the laser Rayleigh scattering using a dichroic mirror (Sem-rock RazorEdge). Then, the Raman scattered light is sent to the spectrometer (right portion of Fig. 2), where it is filtered first using a long pass (edge) filter (Semrock RazorEdge), followed by passing through a volume holographic grating (Wasatch Photonics, $\sim$1000 lines mm^{-1}). This light is then dispersed onto the DMD (Texas Instruments, DLP3000, 608×684 mirror array with 10.8 μm mirror pitch). The spectral window in this system is $\sim$200–4100 cm^{-1}. For all data collected in this paper, we binned two columns of adjacent DMD mirrors together, yielding a total of 342 "bins" with each energy bin corresponding to $\sim$12 cm^{-1}. Light from the DMD is then focused onto a photon-counting photomultiplier tube (PMT) (Hamamatsu model #H10682-01) with a dark count rate of $\sim$500 photons s^{-1}. TTL pulses from the PMT are counted using a USB data acquisition (DAQ) card (National Instruments, USB-6212BNC). The system is controlled with interface software written in Labview 2013. Binary filter generation is performed as previously described using Matlab (Matlab 7.13 R2011b) [8]. Data was in some cases further processed and manipulated using Igor Pro 6.04.

3.2. Chemicals used in classification/quantitation

Acetone and benzene were purchased from Macron (batch #0000070736) and OmniSolv (lot #42282), respectively. Hexanes were acquired from Baxter (lot #901141). Methylcyclo-hexane was acquired from Mallinckroft (lot #1906 KCBN). Aniline and toluene were acquired from Aldrich (batch #05925CB) and Mallinckroft (lot #8608 X14752), respectively. Aniline was purified via distillation by heating aniline to 190° C in a round bottom flask, which was connected to a chilled condenser. Ethanol was acquired from Koptec (200 Proof, lot #225411) and water was ultrapurified in our lab (Milli-Q UF Plus, 18.2 mΩ cm, Millipore). The overhead
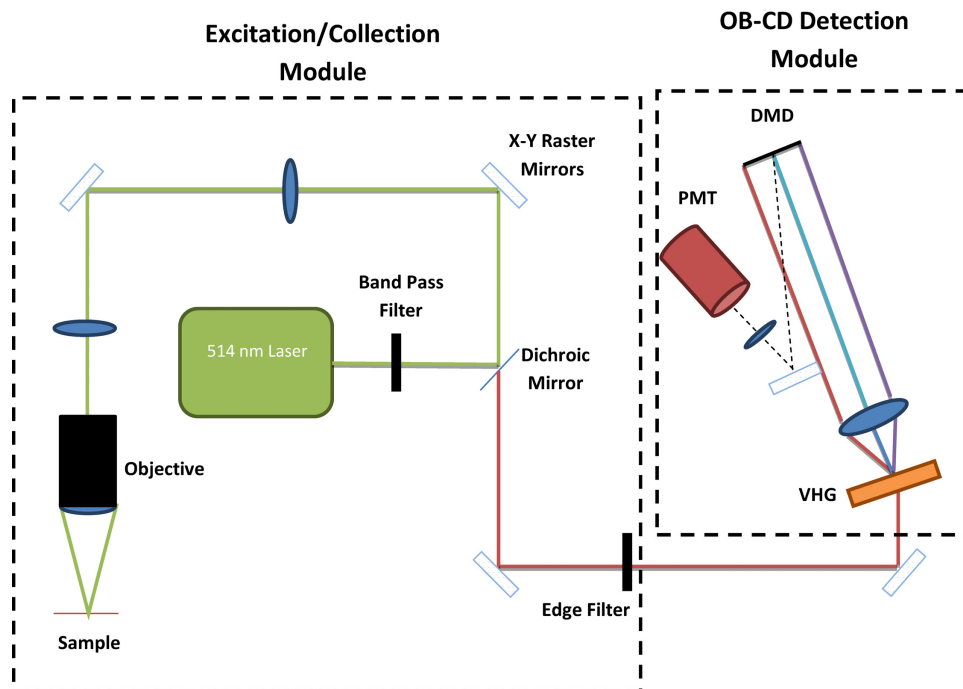
Fig. 2. Schematic of the OB-CD Raman system based upon a 514 nm laser excitation source.

transparency was 3M brand (model #PP2500).

4. Results and discussion

4.1. Treatment of nuisance parameters

Here we demonstrate how the OB-CD detection strategy is influenced by whether the photon emission rates of some of the spectra used for training OB-CD filters are treated as nuisance parameters; we designate such spectra as *nuisance spectra*. More specifically, we generated an OB-CD training set containing the spectra of hexane, methylcyclohexane, a spectral feature arising from the NIR objective in the 785 nm OB-CD system, and the four Bernstein polynomials shown in Fig. 1. Using this training set, we calculated two sets of OB-CD filters (explicitly, both the matrix of binary filters, F, and the measurement time matrix, T): one set for which no spectral features were considered to be nuisance spectra and a second set for which the spectral feature arising from the NIR objective and the Bernstein polynomials were considered to be nuisance spectra. The optimal filters turned out to be identical in both cases (although that need not in general be the case), while the measurement time matrices, T, were quite different as shown in Fig. 3. Notice that the OB-CD filters associated with non-nuisance spectra are turned on for longer percentages of the total measurement time relative to OB-CD filters for the same spectral components when no portion of the training set is considered a nuisance spectra.

One might expect that additional time spent measuring the non-nuisance spectra would result in lower variance in the recovered Raman rates for these components. To test this, the two sets of OB-CD filters (and the associated measurement time matrices) shown in Fig. 3 were used to classify hexane and methylcyclohexane (explicitly, there was no added fluorescence in these samples despite including Bernstein polynomials in both OB-CD training sets). Each chemical was measured using each of the sets of OB-CD filters for 1,000 measurement with 10 ms total
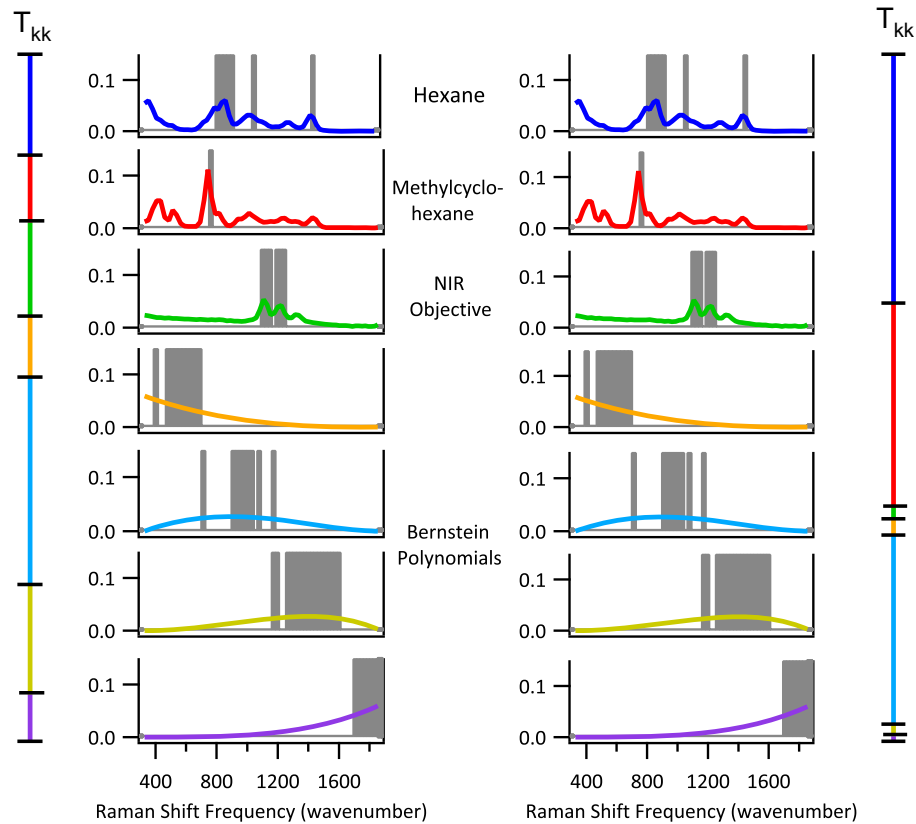
Fig. 3. The colored curves are training spectra (each normalized to unit area) and the gray bands indicate regions in which the OB-CD filters are on (i.e., direct light towards the detector). The Raman spectra were obtained with a spectral resolution of 30 cm^{-1}. The lines labeled T_{kk} correspond to the fraction of the total measurement time that data is collected using the filter associated with each spectral component (denoted by color). The OB-CD filter and T_{kk} results on the left were obtained without considering any components to be nuisance spectra, while those on the right were obtained when considering the NIR objective and Bernstein polynomials to be nuisance spectra.

integration time. The results of these measurements, shown in Fig. 4, clearly reveal the reduced variance (smaller 95% confidence bands) obtained when treating only the two components of interest as non-nuisance spectra. Note in particular that the mean recovered Raman rates for hexane and methylcyclohexane generated from both sets of OB-CD filters differed very little.

4.2. *Validation of Bernstein polynomials*

To test and validate our OB-CD fluorescence suppression strategy we either used a white light source to simulate fluorescence or samples containing fluorescent components. The results described in this section were obtained using a white light illuminator as a convenient fluorescence mimic, as its intensity can readily be varied, and its shape resembles typical fluorescence backgrounds (and has a different shape in the 514 nm and 785 nm spectral region). In subsequent subsections, we describe results obtained using samples with fluorescent impurities, rather than white light, to validate our OB-CD strategy. Here we produced OB-CD filters by training using Bernstein polynomials as well as the Raman spectra of n-hexane and methycyclohexane (and a
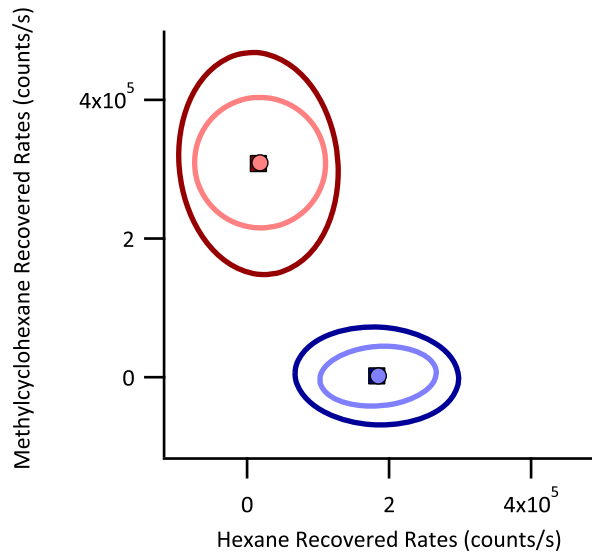
Fig. 4. Recovered Raman rates for hexane (blue) and methylcyclohexane (red) generated using OB-CD filters that considered components of the training set to be nuisance spectra (dark blue and dark red) and OB-CD filters that considered the spectral component arising from the NIR objective and the four Bernstein polynomials to be nuisance spectra (light blue and light red). In all cases, 1,000 OB-CD measurements were taken with a total integration time of 10 ms. The ellipses represent the 95% confidence interval of the recovered Rates for each sample. The large markers in the center of each ellipse represent the mean recovered Raman rates.

spectral component arising from the NIR objective for the 785 nm system). We treat the coefficients of the Bernstein polynomials and the spectral component arising from the NIR objective for the 785 nm system as nuisance parameters. The resulting filters and training spectra from the 785 nm system are virtually identical to those shown in Fig. 3 (and are provided in the Appendix, along with the filters generated for the 514 nm OB-CD system).

The following results were obtained by holding the white light at constant intensity (of about 4 million counts per second) such that the total Raman/fluorescence signal intensity never exceeds 5 million counts per second. We then varied the Raman excitation laser intensity (using neutral density filters) in order to vary the relative amount of Raman and fluorescence in the measured spectra and OB-CD signals, and thus determine how fluorescence background influenced our the recovery of apparent Raman rates using OB-CD.

At each Raman signal intensity, we recovered Raman rates using the OB-CD filters as described in Section 2.1, both with and without the white light background. This allowed us to determine the error in recovered Raman rates as a result of adding fluorescent (white light) background. Figure 5 compares the Raman rates recovered with (*y*-axis) and without (*x*-axis) added white light when using 30 ms total integration time for each measurement. The number at the top indicates the ratio of the integrated area of the fluorescence and Raman signals and the error bars represent the standard deviations of the Raman rates for each component (see the figure caption for further details).

If fluorescence is not perfectly modeled, then the recovered Raman rates can contain a systematic modeling error whose magnitude increases with fluorescent intensity. When using a constant intensity white light to model fluorescence such modeling error introduces an approximately constant offset to the recovered Raman rates. The magnitude of this offset can be de-
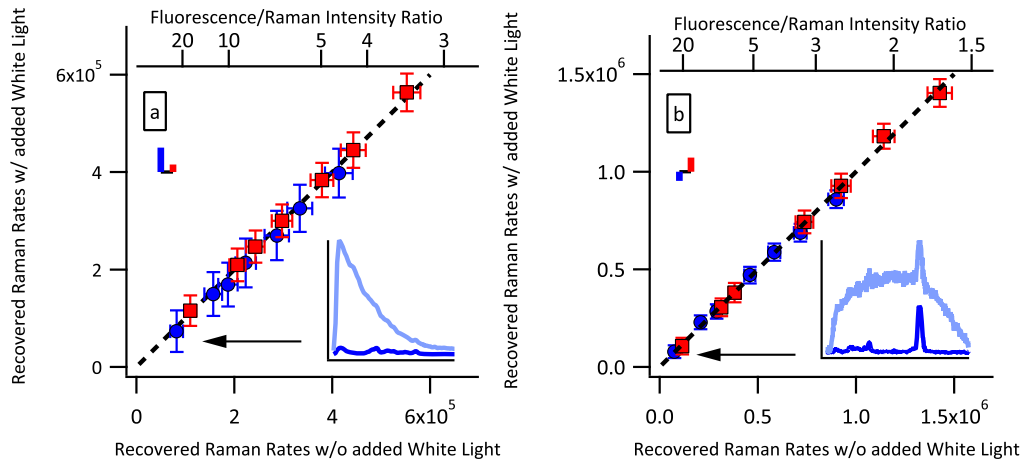
Fig. 5. Plot of hexane (blue) and methylcyclohexane (red) recovered Raman rates measured without added white light versus recovered Raman rates measured with added white light on the (a) 785 nm laser excitation system and (b) 514 nm laser excitation system. Rates have each been corrected by removing a small constant vertical offset (modeling error) whose magnitude was determined by measuring the apparent recovered Raman rates obtained in measurements performed on white light without Raman. The magnitude of this correction is represented by the colored bars in the upper left of each plot. Each point represents the means of 1,000 measurements (each obtained using a 30 ms total integration time) with error bars representing 1 standard deviation. Top axis denotes the ratio of the total (integrated) number of the white light/Raman photons. The inset spectra were obtained from hexane with and without added white light with ∼1 OD neutral density filter and correspond to measurements made at the points denoted by the arrows.

termined by measuring the apparent recovered rates of the Raman components obtained when measuring only white light (containing no Raman photons). For the measurements shown in Fig. 5, these modeling errors were relatively small and have magnitudes indicated by the bars in the upper left of each plot. These modeling errors have been subtracted from each of the points in Fig. 5. In other words, before correcting for this modeling error, all of the recovered Raman rates were slightly offset from the dashed diagonal line (of slope 1).

If the spectrum of white light was modeled perfectly by a degree-three polynomial (or was corrected for modeling error, as described above), we would expect that the mean recovered Raman rates for samples with added white light would not significantly differ from the mean recovered Raman scattering rates without added white light. In other words, we would expect the points to lie on a line with slope one as indicated by the dashed lines in Fig. 5. Thus, the agreement between the points and dashed line in Fig. 5 clearly demonstrate that Raman components can be quantified accurately in the presence of fluorescence backgrounds whose integrated intensity is up to 20 times that of the Raman component of interest. Note that the factor of 20 is obtained from the results shown in Fig. 5, as this is when the Raman signal-to-noise approaches 1:1.

Samples with larger fluorescence/Raman intensity ratios can in principle be accurately analyzed using OB-CD with longer measurement times. However, when the integration time approaches one second it may be appropriate to use conventional full spectral measurements and fluorescence subtraction procedures as the OB-CD strategy is primarily advantageous for performing high speed (or low light level) measurements that are not compatible with CCD detection. Additionally, performing OB-CD measurements on samples in which fluorescence is more than 20 times as intense as the Raman signal of interest would require careful modeling

error correction (as the modeling error would become large relative to the Raman intensities). The results presented in Section 4.3 demonstrate the accuracy with which high speed OB-CD Raman classification and quantitative measurements may be performed without correcting for model error so long as the fluorescence background intensity does not exceed 20 times the Raman signal intensity.

4.3. Raman quantitation and classification of fluorescent samples

4.3.1. Toluene and fluorescent aniline

The following results were obtained using liquid mixtures of toluene and an aniline sample that was partially oxidized and, as a result, developed a fluorescent impurity that could be removed by distillation. We selected these two liquids because of their significant spectral overlap (the dot product of the two normalized spectral vectors is 0.91) and thus successful classification of aniline/toluene mixtures may be used to demonstrate that our fluorescent mitigation strategy is compatible with the Raman-based quantification of such spectrally overlapped mixtures.

We trained OB-CD filters using 785 nm spectra obtained from distilled aniline, toluene, the NIR objective spectrum describe above, as well as the four Bernstein polynomials shown in Fig. 1 (all of the resulting spectra and OB-CD filter functions are given in the Appendix). For this experiment, we treated the spectral component arising from the NIR objective and the four Bernstein polynomials as nuisance spectra. We used OB-CD to recover Raman rates for toluene, distilled aniline, fluorescent aniline, and mixtures of both types of aniline and toluene. Using these recovered Raman rates, we calculated apparent volume fractions of aniline and toluene as follows:

$$\chi_i = \frac{w_i \hat{\Lambda}_i}{\sum_i w_i \hat{\Lambda}_i},$$

where w_i is equal to $M_i / \hat{\Lambda}_i^{\text{Max}}$, M_i is equal to molarity of the ith pure liquid, and $\hat{\Lambda}_i^{\text{Max}}$ is equal to the mean recovered Raman scattering rate for the ith pure liquid as previously reported [9]. We then estimated the apparent volume fraction (Φ) for aniline and toluene in each sample. We did this by dividing the apparent mole fraction (for either aniline or toluene) by the molarity of each pure liquid as follows:

$$\Phi_i = \frac{M_i \chi_i}{\sum_i M_i \chi_i}.$$

Figure 6 plots the resulting apparent volume fractions of toluene and aniline as well as mixtures of the two. The results in Fig. 6 demonstrate that the mean recovered Raman rates are insensitive to the fluorescence arising from the impure aniline sample. The variance of the measurements without fluorescence, however, is less than the variance of samples with fluorescence (as a result of additional shot noise in the latter measurements).

4.3.2. Aqueous ethanol and fluorescent tequila

Previous work [22, 23] has demonstrated that Raman spectroscopy can be used to quantify the volume percentage of ethanol in tequila samples and qualitatively distinguish distilled ("silver") and highly fluorescent, aged (or "golden") tequilas, even in the presence of fluorescence (more common in aged, so-called "golden" tequila). Here we show that our OB-CD fluorescence mitigation strategy can be used to quantify the volume percentage of ethanol in tequila, even for fluorescent "golden" tequila samples at speeds much greater than those previously reported for this application.

We used the 514 nm laser-based OB-CD system for these studies, both because there was more fluorescence produced at this wavelength than when using the 785 nm excitation and be-cause the C-H and O-H stretch vibrational bands are not readily detectable using the 785 nm
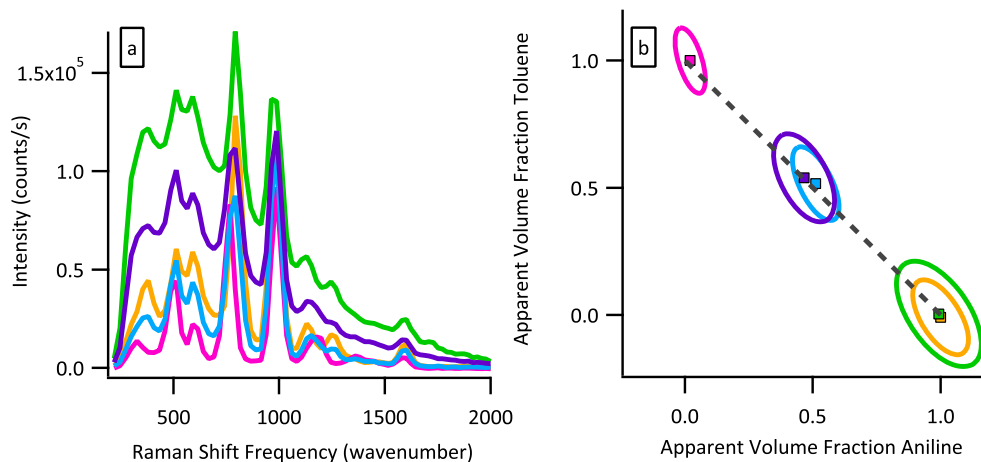
Fig. 6. (a) Spectra of distilled aniline (orange), toluene (magenta), fluorescent aniline (green), a 47:53 volume-by-volume mixture of distilled aniline and toluene (dark green), and a 52:48 mixture of fluorescent aniline and toluene (cyan) measured on the 785 nm OB-CD system. (b) Apparent volume fractions of distilled aniline (orange), toluene (magenta), fluorescent aniline (green), a 47:53 volume-by-volume mixture of distilled aniline and toluene (dark green), and a 52:48 mixture of fluorescent aniline and toluene (cyan). Each chemical was sampled 1,000 times at 20 ms per experiment. Ellipses correspond to the 95% confidence interval of the recovered rates for each sample. The large squares with black borders in the center of each ellipse represent the mean of each sample.

system. Spectra were collected and OB-CD filters were trained using ethanol, water, and Bernstein polynomials (shown in the Appendix). Note that we treated the four Bernstein polynomials as nuisance spectra for OB-CD filter generation. After this, OB-CD was used to recover Raman rates for ethanol and water in a silver tequila ("Arandas" brand) and a golden tequila ("Casamigos" brand). The corresponding apparent volume fractions were obtained from the recovered rates as shown in Fig. 7. In order to keep the fluorescence photon rates within the linear regime of the PMT detector, the laser intensity at the sample was reduced to ∼2 mW using a neutral density filter placed in front of excitation laser and the integration time per sample was increased to 100 ms.

The inset table in Fig. 7(b) shows the mean apparent ethanol volume fractions obtained in a measurement times of 100 ms and, parenthetically, the label volume percent ethanol for each sample. As can be seen, our predicted volume percentages of ethanol very nearly match the label percentage. However, the variance of the fluorescent "golden" tequila measurements is much greater than that of the "silver" tequila measurements due to the increased shot noise resulting from the fluorescence background. In spite of this, we note that by using OB-CD, we can accurately predict the volume percentage of ethanol in tequila samples even when the integrated intensity of the fluorescence of the sample is 20 times larger than the integrated Raman signal. Since the signal-to-noise of such measurements is typically limited by photon (shot) noise rather than read noise, the total time required to obtain a given precision depends on the available laser power and thus is expected to be comparable to that obtained using full spectral measurements (under otherwise identical conditions).

4.3.3. Fluorescent plastic film photobleaching

Here we show an imaging application of our OB-CD fluorescence modeling technique to demonstrate that the recovery of Raman scattering rates is unaffected by fluorescence pho-
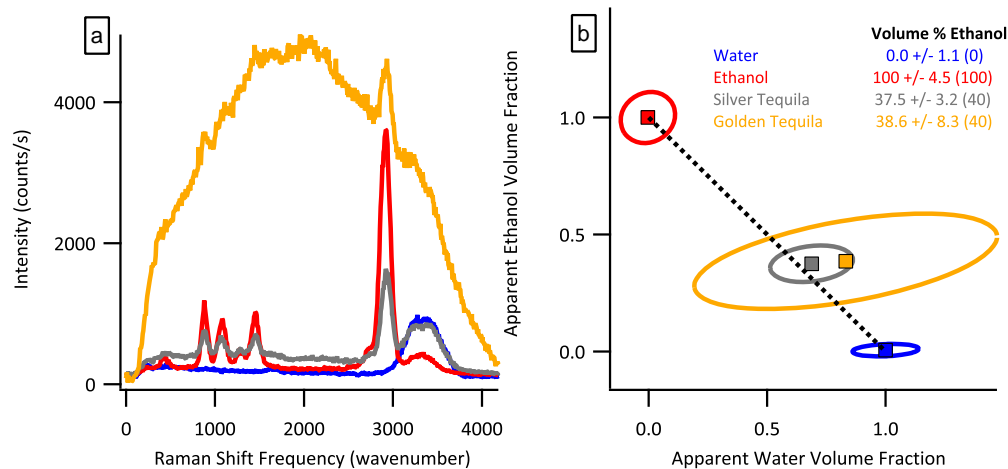
Fig. 7. (a) Spectra of water (blue), ethanol (red), Arandas brand silver tequila (gray), and Casamigos brand golden tequila (dark yellow) measured on the 514 nm OB-CD system (b) Apparent volume fractions of water (blue), ethanol (red), silver tequila (gray), and golden tequila (dark yellow) are compared with the nominal volume fractions (as obtained from the label on the tequila bottles). Each chemical was sampled 1,000 times at 100 ms per OB-CD measurement. Ellipses correspond to the 95% confidence interval of the recovered rates for each sample. Large squares with black borders represent the mean of each sample. The dashed line corresponds to line with slope −1. Inset table reports the mean apparent volume fraction of ethanol (plus/minus 1 standard deviation) for each sample and then, parenthetically, the label ethanol volume percentage for each sample.

tobleaching. For this purpose, we used a plastic film sample consisting of a clear overhead transparency of ∼1.7 mm thickness. This sample was chosen as it was found to contain both Raman and fluorescence signals when excited at 785 nm and the fluorescence could be photobleached by exposure to the excitation laser. Additionally, the film exhibited fluorescence with an integrated intensity 10 times that of the integrated intensity Raman features.

While photobleaching decreased the fluorescence background intensity of the sample by ∼50%, the remaining fluorescence could not readily be further photobleached. Thus, for OB-CD training purposes, we generated a Raman spectrum of the plastic by manually performing a polynomial background subtraction from a spectrum of photobleached plastic in the 328 nm^{-1} to 2057 nm^{-1} region. More specifically, the polynomial subtraction was performed using the "backcor" MATLAB algorithm (Vincent Mazet, 2010), using an Asymmetric Huber cost function, a threshold of 0.01, and four third-degree Bernstein polynomials as a basis. The resulting background subtracted Raman spectrum, as well as the spectra of the overhead transparency before and after photobleaching are shown in Fig. 8.

Next, OB-CD filters were calculated by training on the fluorescence-subtracted Raman features of the plastic film, the spectral component arising from the NIR objective, and the four third-degree Bernstein polynomials (and the resulting training spectra are provided in supplementary material). Note that unlike the filters constructed for previous examples, no components were considered nuisance spectra when calculating OB-CD filters, as we wanted to accurately estimate the intensity of the fluorescence before and after photobleaching. Using these filters, a 200 pixel × 200 pixel region of the plastic film (approximately 1 mm × 1 mm) was imaged with an integration time of 10 ms per pixel. Once this image was collected, two lines were photobleached in the transparency to form a photobleached "+" pattern near the center of the field of view (as shown in Fig. 10). Each line, consisting of 50 pixels, was photobleached for
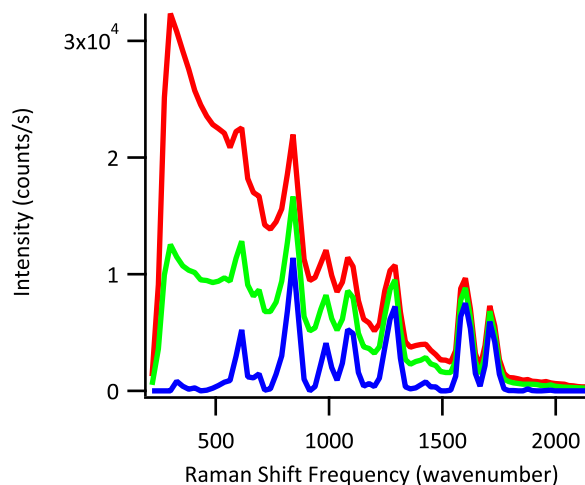
Fig. 8. The measured spectra of a cellulose acetate overhead transparency are plotted before photo-bleaching (red) and after 20 minutes of photobleaching (green). The output of the polynomial baseline subtraction is also plotted (blue).

10 minutes by scanning the laser repeatedly over the "+" pattern at a rate of 1 second per pixel. After photobleaching, the same field of view was reimaged and OB-CD was used to recover the Raman and fluorescence rates. Images were generated using the recovered rates using a method we have previously described [9]. The fluorescence intensity in this image, was determined from the sum of the recovered rates for all four Bernstein polynomials. Note that several spots on the plastic film were highly fluorescent (likely due to a fluorescent impurity, or dust particle, in the film), with counts well outside the linear region of the PMT and a fluorescence background intensity much greater than 20 times the average Raman signal. These pixels also had unusually high recovered apparent Raman rates, which we attributed to model error. These points were removed from the image, as indicated by black dots in the images shown in Fig. 9.

The upper two panels in Fig. 9 show the apparent recovered Raman rates before (left) and after (right) photobleaching, while the lower two panels show the corresponding apparent recovered fluorescence rates. Note that there is no evidence of a "+" pattern in the upper right panel; this indicates that photobleaching did not alter the apparent recovered Raman rates obtained from the film. There was a small ($\sim$10%) decrease in average fluorescence intensity after photobleaching. We attributed this to the photobleaching that occurred while scanning the laser over the entire region during the OB-CD measurement. The similarity of the two upper images in Fig. 9 clearly demonstrates that we are able to obtain high-speed Raman intensity measurements in the presence of a fluorescent background with variable intensity.

5. Conclusions

We have demonstrated an OB-CD fluorescence mitigation strategy that can be used to accurately recover Raman rates from samples with moderate fluorescence intensity (that is, up to 20 times more intense than that of the integrated Raman signal). These results were achieved by quantifying fluorescence using OB-CD filters trained on cubic Bernstein polynomials. We have validated this strategy using both white light as a fluorescence mimic, as well as using fluorescent liquid and solid samples. Thus, the present results demonstrate the feasibility of fast (sub-second) OB-CD based Raman classification and quantitation of moderately fluorescent
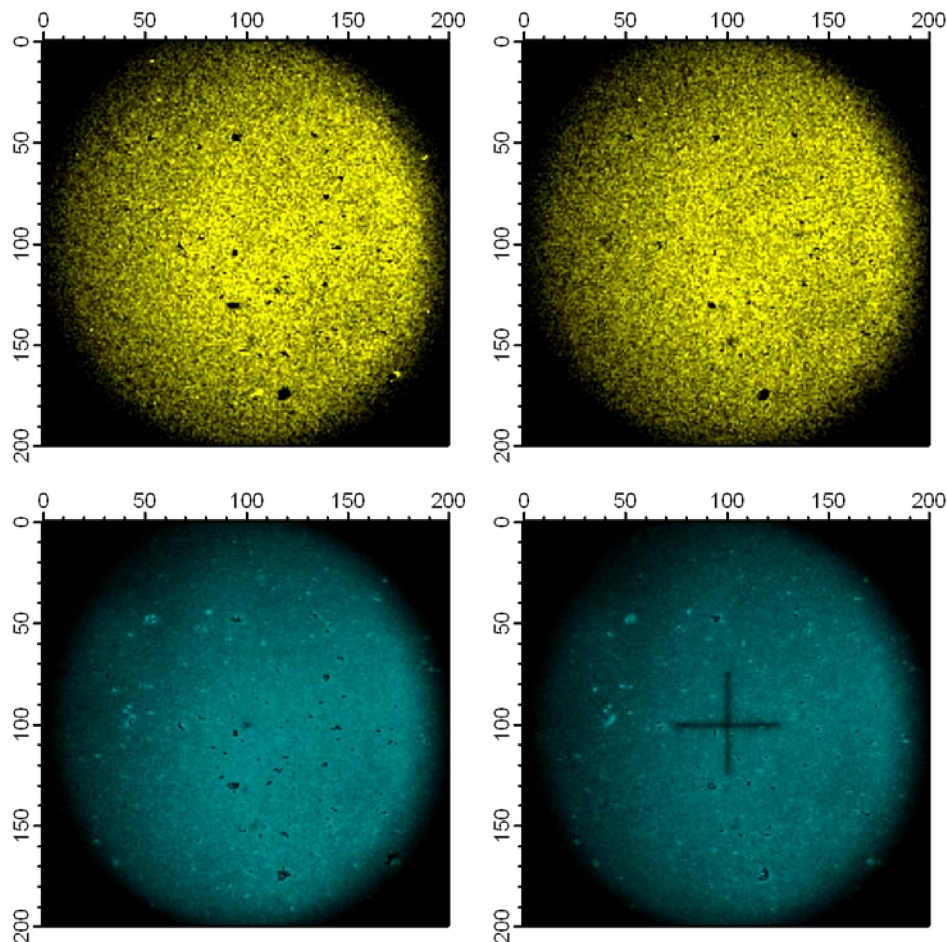
Fig. 9. Images showing the recovered Raman (yellow) and fluorescence (cyan) rates of a cellulose acetate overhead transparency before (images on the left) and after (images on the right) photobleaching a "+" pattern into the center of the imaged area. All images were collected with an integration time of 10 ms per pixel. The circular nature of these images arises from the field of view of the objective, as the images were obtained by raster-scanning the angle of the laser as it enters the back of the objective (while remaining centered in the objective).

samples. This approach can be extended to systems with a fluorescence/Raman intensity ratios greater than 20:1, but would likely require turning down the laser intensity (to avoid detector saturation) and using much longer integration times. Thus, the presented OB-CD strategy is expected to be most useful in applications requiring fast analysis of liquid and solid samples whose fluorescence does not overwhelm the underlying Raman chemical fingerprints. This is consistent with previous results [10], which indicated that the trade-off between higher read-noise and higher spectral information content of full-spectral CCD measurements relative to the OB-CD detection strategy would indicate that OB-CD is most advantageous (relative to CCD measurements) in fast (low-signal) applications that unaccessible to CCD-based measurements.

6. Appendix

Fig. 10 shows the training spectra and calculated OB-CD filters for several of the samples in this paper.
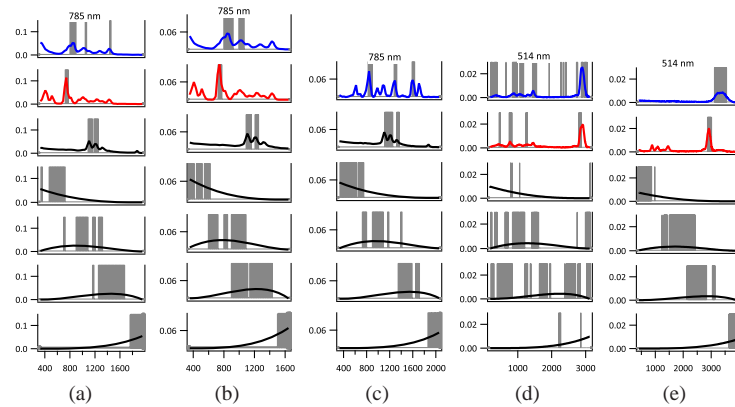
Fig. 10. Area-normalized spectra plotted against Raman shift frequency (wavenumber) shown here pertain to results obtained using a 785 nm and 514 nm excitation laser as noted above each subfigure. Note that the 785 nm spectra were measured with a resolution of 30 cm^{-1} and the 514 nm spectra were measured with a resolution of 12 cm^{-1}. Unless otherwise noted, the spectral component arising from the NIR objective and the Bernstein polynomials were always considered nuisance spectra. (a) Spectra and the resulting OB-CD filters for (in order from top down): n-hexane, methylcyclohexane, the spectral component arising from the NIR objective and the four degree-three Bernstein polynomials. The fraction of the total measurement time that each filter was collecting was 0.385, 0.219, 0.055, 0.034, 0.268, 0.031, and 0.009, respectively. (b) Spectra and the resulting OB-CD filters for (in order from top down): n-hexane, methylcyclohexane, and the four degree-three Bernstein polynomials. The fraction of the total measurement time that each filter was collecting was 0.248, 0.388, 0.010, 0.032, 0.277 and 0.045, respectively. (c) Spectra and the resulting OB-CD filters for (in order from top down): aniline, toluene, spectral component arising from the NIR objective, and the four degree-three Bernstein polynomials. The fraction of the total measurement time that each filter was collecting was 0.484, 0.265, 0.025, 0.003, 0.154, 0.059 and 0.010, respectively. (d) Spectra and the resulting OB-CD filters for (in order from top down): ethanol, water, and the four degree-three Bernstein polynomials. The fraction of the total measurement time that each filter was collecting was 0.276, 0.261, 0.027, 0.116, 0.232, and 0.088 , respectively. (e) Spectra and the resulting OB-CD filters for (in order from top down): Raman features of the plastic film, the spectral component arising from the NIR objective, and the four degree-three Bernstein polynomials. The fraction of the total measurement time that each filter was collecting was 0.099, 0.210, 0.099, 0.271, 0.212, and 0.109, respectively. No components were considered nuisance spectra, as we wanted to accurately estimate the intensity of the fluorescence before and after photobleaching.

Acknowledgments